Kukkola, Jarno; Hinkkanen, Marko

Method for DC-link capacitance identification in voltage-source converters

Published in:
The 23rd International Symposium on Power Electronics, Electrical Drives, Automation and Motion

DOI:
10.1109/SPEEDAM.2016.7525833

Published: 22/06/2016

Document Version
Peer-reviewed accepted author manuscript, also known as Final accepted manuscript or Post-print

Please cite the original version:
Kukkola, J., & Hinkkanen, M. (2016). Method for DC-link capacitance identification in voltage-source converters. In *The 23rd International Symposium on Power Electronics, Electrical Drives, Automation and Motion* (pp. 34-40). (International Symposium on Power Electronics, Electrical Drives, Automation and Motion). IEEE. https://doi.org/10.1109/SPEEDAM.2016.7525833

Method for DC-link Capacitance Identification in Voltage-Source Converters

Jarno Kukkola and Marko Hinkkanen
Aalto University, Department of Electrical Engineering and Automation
P.O. Box 13000, FI-00076 Aalto, Finland

***Abstract*—A DC-link capacitance estimation method is presented for a three-phase voltage-source converter. The measured phase currents and DC-link voltage of the converter are used in formulation of the input and output signals for the estimator. The estimator is based on the ordinary least squares method. The capacitance can be estimated during the startup of the converter or while the converter is in normal operation. The proposed method is experimentally validated and the results indicate that the capacitance value is estimated with a good accuracy.**

***Index Terms*—Active-front-end rectifier, capacitance estimation, condition monitoring, DC-link capacitor, grid-connected converter.**

I. Introduction

Voltage-source grid-connected converters are widely used for AC-to-DC and DC-to-AC power conversion in various applications, such as electric motor drives, electric vehicles, and renewable energy generation. The DC-link capacitors or capacitor banks of these converters play an important role working as an energy buffer and balancing the DC voltage variations. However, among the semiconductor devices the capacitors are the most fragile components in the converters [1]. A typical reason for the capacitor failure is the long-term wear out, which can be seen as a change of electrical parameters of the capacitor [2], [3]. Monitoring electrical parameters of the capacitor provides information of the capacitor condition. Moreover, the appropriate time to replace the capacitor might be predicted before the failure.

Condition of the capacitor can be monitored by estimating or measuring the capacitance, which is typically reduced at the end of the lifetime [3]. In the case of aluminium electrolytic capacitors, also increased equivalent series resistance (ESR) has been used as an end-of-life indicator [2]. However, the capacitance-monitoring method is more universal, since it is applicable in the case or metallized polypropylene film capacitors and multi-layer ceramic capacitors as well [3]–[6].

In the literature, various methods for estimation of the DC-link capacitance have been presented [4]–[13]. In the case of motor drives, the capacitance has been estimated by discharging the capacitor energy to the stator winding when the motor is stopped [6], [9], [13]. Estimation has been based on the change of the charge that is proportional to the capacitance and the change in the voltage. However, these methods cannot be used in the applications where the motor does not exist, e.g, solar inverters. Alternatively, the discharge has been generated by a braking circuit [4]. In [11], the capacitance is estimated by monitoring the decreasing voltage together with the discharge time when the capacitor bank energy is discharged through the trimming resistors.

During the converter operation, the capacitance and ESR have been estimated using the ripple voltage and current of the capacitor as input signals for the Kalman filter [12]. The ripple-voltage based method has also been proposed in [5] and [14]. The drawback of the ripple-voltage based methods is that the measurement system, including sensors, should have a high bandwidth in order to capture ripple waveforms originating from the pulse-width modulation [5].

Another online approach is to inject a low-frequency sinusoidal signal into the power-producing component of the converter current reference [7]. The injection signal causes low-frequency oscillations in the converter power and further in the DC-voltage. In order to estimate the capacitance, the oscillatory component of the DC-voltage has been used together with the capacitor current as inputs for a recursive-least-squares algorithm [7]. Alternatively, a low-frequency sinusoidal signal has been injected into the reference of the DC-link voltage controller [8] or the torque-producing current component in the case of motor drives [10] for capacitance estimation. The low-frequency injection-based methods have been shown to provide accurate estimates for the capacitance. However, the control system has to be significantly modified for sinusoidal signal injection and in order to obtain band-pass-filtered data for the estimation algorithm.

If the capacitance estimate is used in condition monitoring, the temperature of the capacitor during the estimation must be considered, since the capacitance value can be highly dependent on temperature [8], [9], [12]. Besides the condition monitoring, the estimated capacitance value is useful in the control tuning. In multi-drive systems, e.g., [15], several inverters are connected into a common DC-link and an active-front-end rectifier is regulating the DC-link voltage. In these systems, the capacitance of the DC-link can vary significantly, if the number of the inverters connected to the common DC-link is changing. The varying capacitance changes the system dynamics and may cause troubles for DC-link voltage control and the system stability. Therefore, the real-time estimation of the DC-link capacitance is very valuable enabling real-time adjustment of the controller parameters.

In this paper, a DC-link capacitance identification method is presented. An excitation signal for identification is fed into the converter current or power reference. The capacitance is

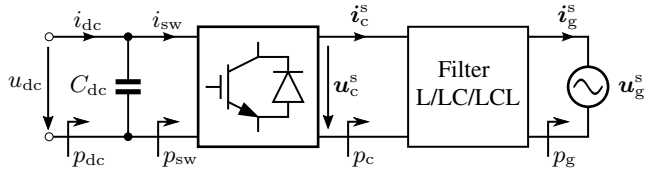

Fig. 1. Power flow diagram of a grid-connected converter.

estimated using the measured DC-link voltage and calculated capacitor energy as input signals for a least-squares estimator. The proposed method can be implemented in a typical grid-connected converter, e.g., solar inverter, that has the DC-link voltage and converter phase current measurements. No hardware modifications are needed, and only minor changes in the converter control software are required. Moreover, the estimation of the capacitance can be carried out during the normal operation or at the startup of the converter. The proposed method is experimentally validated using a 12.5-kVA grid-connected converter.

II. System Model

A. Power Flow

Fig. 1 shows a power flow diagram of a grid-connected converter equipped with a grid-side filter. The both power directions are possible, and the positive power direction is selected to correspond to the inverter operation mode. The external power supplied into the DC-link is

$$p_{\mathrm{dc}} = u_{\mathrm{dc}} i_{\mathrm{dc}} \tag{1}$$

where u_{dc} is the DC-link voltage and i_{dc} is the external direct current. The power fed into the grid is p_{g}. The switching-cycle averaged quantities are assumed and complex-valued space vectors are used (marked with boldface symbols). The converter output power is

$$p_{\mathrm{c}} = \frac{3}{2}\,\mathrm{Re}\{\boldsymbol{u}_{\mathrm{c}}^{\mathrm{s}} \boldsymbol{i}_{\mathrm{c}}^{\mathrm{s}*}\} = \frac{3}{2}\,\mathrm{Re}\{\boldsymbol{u}_{\mathrm{c}} \boldsymbol{i}_{\mathrm{c}}^{*}\} \tag{2}$$

where $\boldsymbol{u}_{\mathrm{c}}^{\mathrm{s}}$ is the converter voltage and $\boldsymbol{i}_{\mathrm{c}}^{\mathrm{s}}$ is the converter current in stationary coordinates and $\boldsymbol{u}_{\mathrm{c}}$ and $\boldsymbol{i}_{\mathrm{c}}$ are the corresponding quantities in synchronous coordinates. The complex conjugate is denoted by superscript *. On the DC-side of the semiconductor bridge, the power is

$$p_{\mathrm{sw}} = p_{\mathrm{c}} + p_{\mathrm{l}}, \tag{3}$$

where p_{l} represents the losses of the converter.

The measured converter voltage is not typically available. Thus, the converter-voltage reference $\boldsymbol{u}_{\mathrm{c,ref}}^{\mathrm{s}}$, produced by a control algorithm, is used in power calculation. Due to the finite computation time in a practical system, the reference $\boldsymbol{u}_{\mathrm{c,ref}}^{\mathrm{s}}$ calculated at t is applied to the system at the next sampling interval $t + T_{\mathrm{s}}$, where T_{s} is the sampling time. In other words, the voltage is modeled as $\boldsymbol{u}_{\mathrm{c}}^{\mathrm{s}}(t) = \boldsymbol{u}_{\mathrm{c,ref}}^{\mathrm{s}}(t - T_{\mathrm{s}})$. Then, the power can be expressed

$$p_{\mathrm{c}}(t) = \frac{3}{2}\,\mathrm{Re}\{\boldsymbol{u}_{\mathrm{c,ref}}^{\mathrm{s}}(t - T_{\mathrm{s}}) \boldsymbol{i}_{\mathrm{c}}^{\mathrm{s}*}(t)\} \tag{4}$$

B. DC-link Capacitor

Assuming an ideal DC-link capacitor, the dynamics of the DC-link voltage are

$$C_{\mathrm{dc}} \frac{\mathrm{d}u_{\mathrm{dc}}}{\mathrm{d}t} = i_{\mathrm{dc}} - i_{\mathrm{sw}} \tag{5}$$

where C_{dc} is the capacitance and i_{sw} is the current fed to the converter. The capacitance is assumed to be constant during a short observation period. Multiplying both sides of (5) by u_{dc}, the capacitor-energy dynamics are obtained

$$\frac{\mathrm{d}}{\mathrm{d}t} \underbrace{\left(\frac{1}{2} C_{\mathrm{dc}} u_{\mathrm{dc}}^2\right)}_{W} = p_{\mathrm{dc}} - p_{\mathrm{sw}} \tag{6}$$

where

$$W = \frac{1}{2} C_{\mathrm{dc}} u_{\mathrm{dc}}^2 \tag{7}$$

is the energy stored in the capacitor. In the integral form, the energy is

$$W(t) = \int [p_{\mathrm{dc}}(t) - p_{\mathrm{sw}}(t)]\mathrm{d}t + W_0 \tag{8}$$

where W_0 is the initial energy stored in the capacitor at $t = 0$.

Assume that the powers p_{dc}, p_{sw}, and p_{c} are observed between $0 \le t \le t_{\mathrm{e}}$, where t_{e} is the end time of the observation period. Initial values at the beginning of the observation period ($t = 0$) are marked with the subscript '0'. If the constant external power $p_{\mathrm{dc}}(t) = p_{\mathrm{dc0}}$ is assumed during $0 \le t \le t_{\mathrm{e}}$ and the capacitor losses are minor $p_{\mathrm{dc0}} - p_{\mathrm{sw0}} \approx 0$, the external power can be written $p_{\mathrm{dc}}(t) \approx p_{\mathrm{sw0}}$. Moreover, considering (3), the external power becomes $p_{\mathrm{dc}}(t) = p_{\mathrm{c0}} + p_{\mathrm{l0}}$, where p_{c0} and p_{l0} are the initial converter and loss powers, respectively. Then, together with (3), the energy of the capacitor can be written

$$W(t) = \int [p_{\mathrm{c0}} + p_{\mathrm{l0}} - p_{\mathrm{c}}(t) - p_{\mathrm{l}}(t)]\mathrm{d}t + W_0, \quad 0 \le t \le t_{\mathrm{e}} \tag{9}$$

Furthermore, assuming constant converter losses $p_{\mathrm{l}}(t) = p_{\mathrm{l0}}$ during $0 \le t < t_{\mathrm{e}}$, the equation is simplified

$$W(t) = \int [p_{\mathrm{c0}} - p_{\mathrm{c}}(t)]\mathrm{d}t + W_0, \quad 0 \le t \le t_{\mathrm{e}} \tag{10}$$

The assumption of the constant converter losses is not needed, if the loss variation $p_{\mathrm{l0}} - p_{\mathrm{l}}(t)$ is known as a function of the converter power or current.

For the identification of the capacitance, the energy difference $\Delta W = W - W_0$ is introduced. The energy difference obtained from (7) is

$$\Delta W(t) = \frac{1}{2} C_{\mathrm{dc}} [u_{\mathrm{dc}}^2(t) - u_{\mathrm{dc0}}^2] \tag{11}$$

where u_{dc0} is the capacitor voltage at $t = 0$. On the other hand, the integral (10) directly gives

$$\Delta W(t) = \int [p_{\mathrm{c0}} - p_{\mathrm{c}}(t)]\mathrm{d}t \tag{12}$$

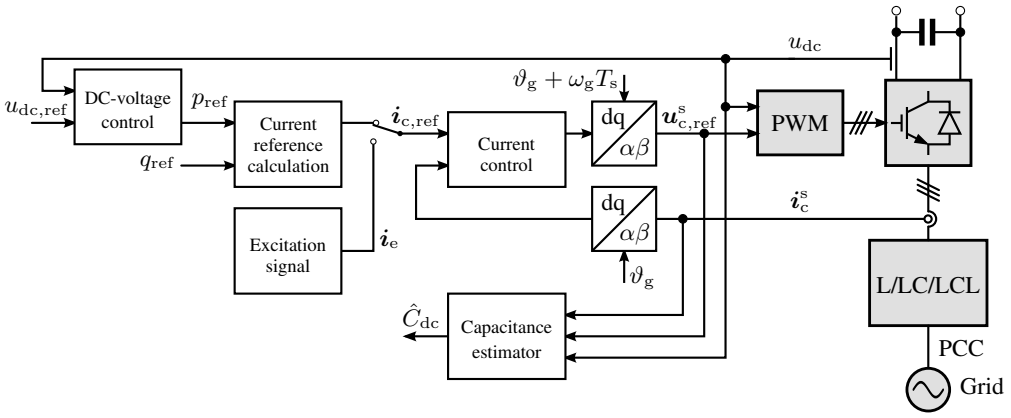

Fig. 2. Control system implemented in the grid-voltage reference frame (ϑ_{g} and ω_{g} are the angle and frequency of the grid voltage, respectively).

Together, the energy differences formulate a linear equation with respect to the variables x and y,

$$C_{\mathrm{dc}} \cdot \underbrace{\frac{1}{2}[u^2_{\mathrm{dc}}(t) - u^2_{\mathrm{dc0}}]}_{y(t)} = \underbrace{\int [p_{\mathrm{c0}} - p_{\mathrm{c}}(t)]\mathrm{d}t}_{x(t)}, \qquad (13)$$

that is the starting point for the identification of the capacitance.

C. Discrete-Time Model

In practical implementation of the converter control, the measured signals are sampled. In addition, they can include noise. Therefore, for identification, the model (13) is extended

$$y(k) = \beta x(k) + v(k) \qquad (14)$$

where

$$y(k) = 0.5[u^2_{\mathrm{dc}}(k) - u^2_{\mathrm{dc0}}] \qquad (15)$$

is the measured output, $x(k)$ is the input, $v(k)$ is a disturbance term, k is the discrete-time index, and $\beta = 1/C_{\mathrm{dc}}$ is the model parameter. The measurement noise is included in $v(k)$. With sampled data, the integral for input signal is calculated using the simple Euler approximation

$$x(k+1) = x(k) + T_{\mathrm{s}}[p_{\mathrm{c0}} - p_{\mathrm{c}}(k)] \qquad (16)$$

where T_{s} is the sampling time.

III. Identification

The identification process is divided into three phases: 1) performing the experiment and data acquisition; 2) estimation of the capacitance; 3) validation of the result. During the experiment and data acquisition, the DC-link voltage u_{dc}, converter voltage $\boldsymbol{u}^{\mathrm{s}}_{\mathrm{c}}$ or its reference $\boldsymbol{u}^{\mathrm{s}}_{\mathrm{c,ref}}$, and converter current $\boldsymbol{i}^{\mathrm{s}}_{\mathrm{c}}$ are stored and the excitation signal $\boldsymbol{i}_{\mathrm{e}}$ is applied.

A. Control System

Cascade control of the DC-link voltage and the converter current is assumed. Fig. 2 shows the control system. Current control can be implemented, e.g., in the grid-voltage-oriented synchronous reference frame. The synchronization can be implemented using conventional (e.g., a phase-locked loop) or sensorless methods (e.g., [16]).

In order to estimate the capacitance C_{dc}, the power p_{c} is disturbed by forcing the converter current reference to be $\boldsymbol{i}_{\mathrm{c,ref}} = \boldsymbol{i}_{\mathrm{e}}$, where $\boldsymbol{i}_{\mathrm{e}}$ is an excitation signal. Alternatively, the excitation signal could be applied into the power reference p_{ref}. During the feed of excitation signal, DC-voltage control is bypassed and the converter is operating in current-control (or power-control) mode.

B. Linear Regression

The input and output signals for the least squares estimation procedure are calculated from (4), (15), and (16). In the identification, the input and output signals are often pre-processed. Removing the means of the input and output signals is recommended for more accurate estimates [17]. The means are

$$\bar{y} = \frac{1}{n}\sum_{k=1}^{n} y(k) \qquad \bar{x} = \frac{1}{n}\sum_{k=1}^{n} x(k) \qquad (17)$$

where n is the number of the collected samples. The input and output signals without means are $x' = x - \bar{x}$ and $y' = y - \bar{y}$, respectively.

The parameter $\beta = 1/C_{\mathrm{dc}}$ is estimated by the ordinary least squares method. The regression problem in vector form is

$$\mathbf{Y} = \beta \mathbf{X} + \mathbf{V} \qquad (18)$$

where $\mathbf{Y} = [y'(1), \ldots, y'(n)]^{\mathrm{T}}$, $\mathbf{X} = [x'(1), \ldots, x'(n)]^{\mathrm{T}}$, and $\mathbf{V} = [v(1), \ldots, v(n)]^{\mathrm{T}}$ is the residual vector. The parameter estimate $\hat{\beta}$ that minimizes the sum of the squared residuals is obtained by least squares method as follows

$$\hat{\beta} = (\mathbf{X}^{\mathrm{T}}\mathbf{X})^{-1}\mathbf{X}^{\mathrm{T}}\mathbf{Y} = \frac{\sum_{k=1}^{n}[x'(k)y'(k)]}{\sum_{k=1}^{n}[x'(k)]^2} \qquad (19)$$

Furthermore, the capacitance estimate is $\hat{C}_{\mathrm{dc}} = 1/\hat{\beta}$.

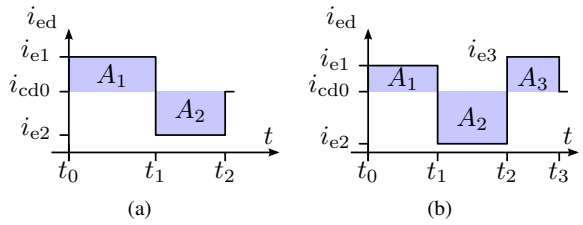

Fig. 3. Real part i_{ed} of an excitation signal $\boldsymbol{i}_{\mathrm{e}}$: (a) two-pulse signal; (b) three-pulse signal. The bias level of the signals is i_{cd0}.

C. Excitation Signal

Since the regressor x' and output signal y' of the parameter estimator (19) are not directly measured, an excitation signal $\boldsymbol{i}_{\mathrm{e}}$, that causes notable changes in x' and y' should be selected. Moreover the variation in x' and y' caused by the excitation signal should be significantly larger than the variation caused by measurement errors including noise. The excitation signal could be, e.g., a multi-sine, random, or pseudo-random binary signal. Here, a simple signal, which is built on rectangular pulses, is selected.

Fig. 3 shows two example signals having two or three pulses of different sizes and lengths. The bias value $\boldsymbol{i}_{\mathrm{e0}} = i_{\mathrm{eq0}} + \mathrm{j}i_{\mathrm{eq0}}$ of the signal is selected to match the initial operating point $\boldsymbol{i}_{\mathrm{c0}} = i_{\mathrm{cd0}} + \mathrm{j}i_{\mathrm{cq0}}$ before the first pulse. The d component of the signal is altered (effectively changing the active power of the converter). The signal is selected to transfer a zero-mean energy difference ΔW around the operating point. Therefore, the two-pulse signal in Fig. 3(a) have equal areas A_1 and A_2. Pulse-lengths ($t_1 - t_0$ and $t_2 - t_1$) and amplitudes (i_{e1} and i_{e2}) are selected to fulfil the area condition and to generate notable changes in x' and y'. In the case of the three-pulse signal shown in Fig. 3(b), the sum of the areas, regarding the bias level i_{cd0}, has to be zero ($A_1 - A_2 + A_3 = 0$) in order to keep the mean of the energy difference zero.

It is to be noted that the selection of the excitation signal is not limited to the presented examples, generally asymmetrical pulses. The pulses can be also symmetrical, and the number of them can vary. The observation time for the identification is the duration of the excitation signal. The main principle for selecting the observation time and the pulse amplitudes is to cause notable changes in x' and y'. Furthermore, if the duration of the excitation signal equals the fundamental period of the grid voltage, the average of the possible fundamental-frequency harmonics becomes zero, e.g., in the measured current.

D. Validation of the Model

The estimator for the output signal is

$$\hat{y}(k) = \hat{\beta} x(k) \tag{20}$$

and the modeling error is

$$e(k) = y(k) - \hat{y}(k) = y(k) - \hat{\beta} x(k) \tag{21}$$

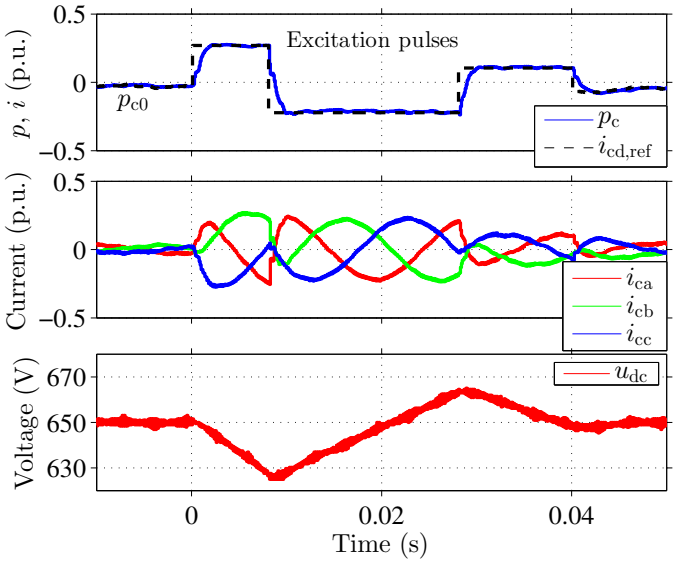

Fig. 4. Measured waveforms of the converter power p_{c}, the phase currents i_{ca}, i_{cb}, and i_{cc}; and the DC-link voltage u_{dc} when a three-pulse excitation signal is applied at the startup of the converter.

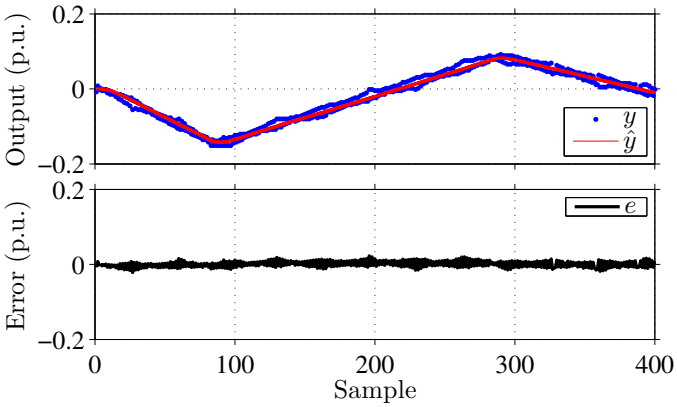

Fig. 5. Measured output signal y, the estimated signal $\hat{y}$, and the modeling error e corresponding to Fig. 4.

A measure for goodness of the estimated linear model is the coefficient of determination [18] that is

$$r^2 = 1 - \frac{\sum_{k=1}^{n} [e(k)]^2}{\sum_{k=1}^{n} [y(k) - \bar{y}]^2} \tag{22}$$

where $0 \leq r^2 \leq 1$. The coefficient describes how well the total variation of the output values $y(k)$ are explained by the model. The coefficient is $r^2 = 1$, if all the values are on the same line $y(k) = \hat{y}(k) = \hat{\beta} x(k)$, e.g., the error terms $e(k)$ are zero. On the other hand, r^2 is zero, if the model does not explain the observed values of y at all.

IV. Experimental Results

The capacitor identification method was experimentally verified. A 12.5-kVA grid-connected converter was used in experiments, and an LCL filter was connected between the converter and the grid. The converter used in tests was loaded by another back-to-back connected grid-connected converter.

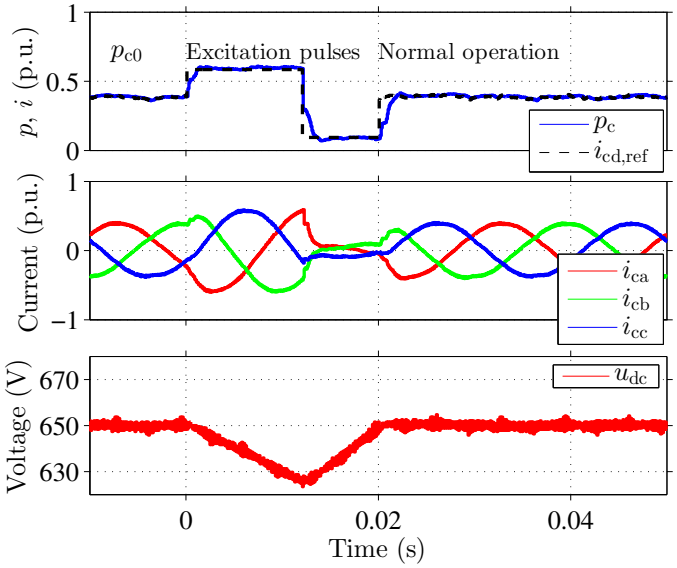

Fig. 6. Measured waveforms of the converter power p_c, the phase currents i_{ca}, i_{cb}, and i_{cc}; and the DC-link voltage u_{dc} when a two-pulse excitation signal is applied. The converter is in normal operation and feeding the power of 5 kW to the grid.

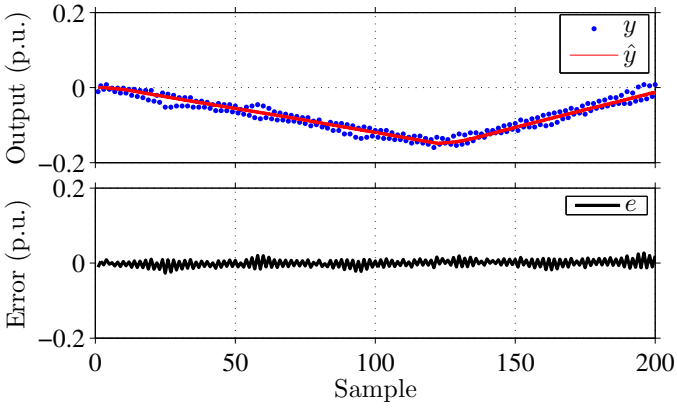

Fig. 7. Measured output signal y, the estimated signal $\hat{y}$, and the modeling error e corresponding to Fig. 6.

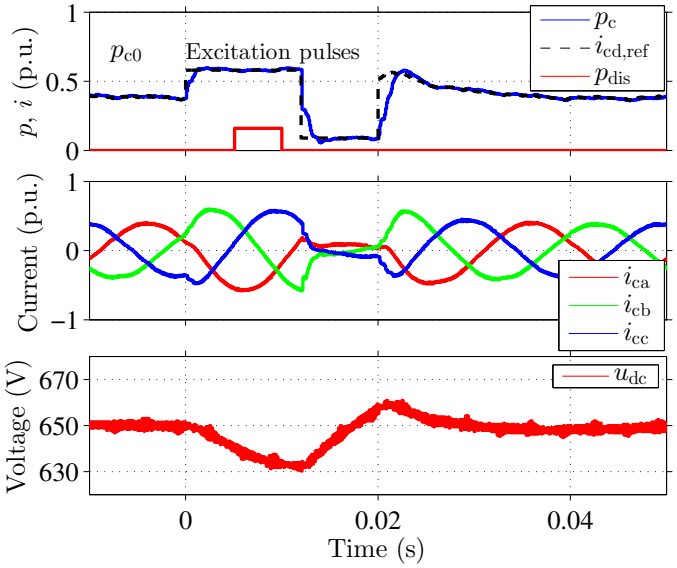

Fig. 8. Measured waveforms of the converter power p_c, the phase currents i_{ca}, i_{cb}, and i_{cc}; and the DC-link voltage u_{dc} when a two-pulse excitation signal is applied. A disturbance p_{dis} is applied in the reference of the loading power p_{dc} at $t = 5 \ldots 10$ ms.

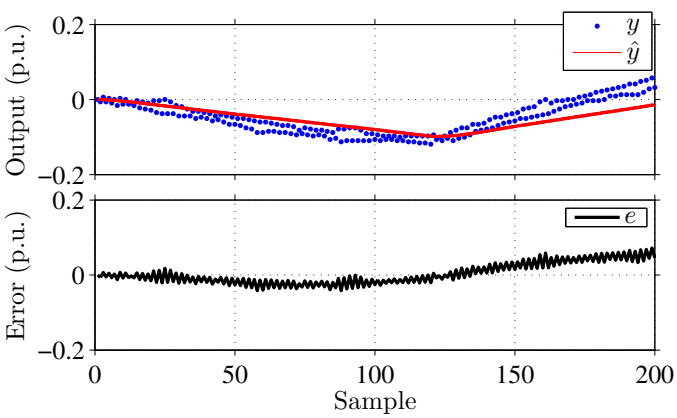

Fig. 9. Measured output signal y, the estimated signal $\hat{y}$, and the modeling error e corresponding to Fig. 8.

The proposed method and converter control software was running on the dSPACE DS1006 processor board. The sampling of the measured signals was synchronized with the pulse-width modulator (PWM). The samples are taken in the beginning and middle of the PWM carrier [19].

A. No-Load Operation

First, the identification method was tested when the converter was not loaded, but it was rectifying the power covering the system losses. Fig. 4 shows the converter current reference $i_{cd,ref}$, calculated power p_c, phase currents, and DC-link voltage when a three-pulse excitation signal was applied at $t = 0$. The excitation signal was generated following the guidelines given in Section III-C. Referred to the initial point i_{cd0}, amplitudes of the pulses were $i_{e1} = 7.5$ A, $i_{e2} = -5$ A, and $i_{e3} = 3.3$ A [cf. Fig. 3(b)]; and the lengths of the pulses were 80, 200, and 120 samples, respectively. The length of the resulting excitation signal was $n = 400$ samples, which equals two periods of the grid voltage. The sampling time was 100 μs corresponding to the sampling frequency of 10 kHz. The switching frequency was 5 kHz.

Data for calculating the output signal y and the regressor signal x were collected during the feed of the excitation signal $\boldsymbol{i}_e$. Before applying $\boldsymbol{i}_e$, the initial power of the converter p_{c0} was calculated and the initial DC-link voltage u_{dc0} was recorded. The values for p_{c0} and u_{dc0} were calculated by taking the mean of the last two samples before the feed of $\boldsymbol{i}_e$.

After the data acquisition, the capacitance estimate $\hat{C}_{dc} = 1/\hat{\beta}$ was calculated using (19). The resulting capacitance is 1.86 mF while the reference value obtained with an RLC meter (Philips PM6304) is 1.83 mF. The reference value was measured at 100 Hz.

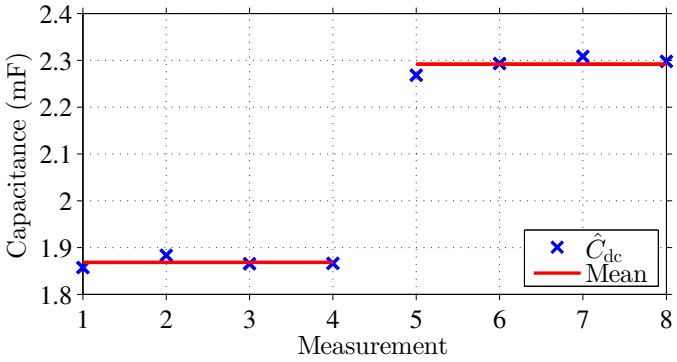

Fig. 10. Estimated capacitance.

Fig. 5 shows the actual output y and the estimated output $\hat{y}$ calculated with (20). Furthermore, the modeling error $e = y - \hat{y}$ (21) is illustrated. As the figure shows, the estimated output predicts well the measured behavior. Moreover, 98.2% of the measured variation in the output variable y is explained by the estimated model ($r^2 = 0.982$).

B. Identification Under Constant Load

The capacitance identification test was repeated during the normal operation of the converter. The converter was feeding the power of 5 kW to the grid, when the excitation signal was applied. Fig. 6 shows the converter current reference $i_{\mathrm{cd,ref}}$, calculated power p_{c}, phase currents, and DC-link voltage when a two-pulse excitation signal was applied. Referred to the initial point i_{cd0}, amplitudes of the pulses were 5 A and -7.5 A [cf. Fig. 3(a)], and the lengths of the pulses were 120 and 80 samples, respectively. The length of the resulting excitation signal was $n = 200$ samples, which equals a period of the grid voltage. The excitation signal was generated following the guidelines given in Section III-C.

After the data acquisition and calculation of the regressor and output signals, the capacitance estimate $\hat{C}_{\mathrm{dc}} = 1/\hat{\beta}$ was calculated using (19). The resulting capacitance is 1.87 mF that is well in line with the result of no-load operation and the reference value (1.83 mF) measured with the RLC meter. Fig. 7 shows the actual output y and the estimated output $\hat{y}$ calculated with (20). Furthermore, the figure shows the modeling error $e = y - \hat{y}$. As the figure illustrates, the estimated output predicts well the measured behavior. Moreover, 93.8% of the measured variation in the output variable y is explained by the estimated model ($r^2 = 0.938$).

C. Varying Load Power

The capacitance identification was tested under varying load power p_{dc} intentionally violating the assumption of constant load power (cf. Section II-B). Fig. 8 shows the converter current reference $i_{\mathrm{cd,ref}}$, calculated power p_{c}, phase currents, and DC-link voltage. During the identification, the disturbance of $p_{\mathrm{dis}} = 2$ kW was applied in the reference of the load power p_{dc} at $t = 5 \ldots 10$ ms. Contrary to the corresponding identification during the constant load (cf. Fig. 6), the DC-link voltage is not returning to its initial value at the end of the excitation pulses $t = 0.02$ s, since the disturbance p_{dis} causes nonzero energy difference ΔW around the operating point. However, the converter is returning to the normal operation (DC-link control is activated) after $t = 0.02$ s, and the DC-link voltage returns back to its initial level around $t = 0.04$ s. Moreover, the estimated capacitance under varying load is biased (2.89 mF), which is also indicated by the non-zero modeling error $e = y - \hat{y}$ that is shown in Fig. 9.

In order to detect failed experiments and to validate the estimation result, the coefficient of determination (22) was introduced. In the case of the varying load power (Figs. 8 and 9) the coefficient is $r^2 = 0.581$. The low r^2 value, in comparison with the result in Section IV-B, indicates that the proposed linear model can not explain the relationship between x and y well, i.e., the coefficient indicates that the estimation result is not correct.

D. Increased Capacitance

The ability to detect capacitance changes was tested by adding an extra capacitor bank of 410 μF to the DC-link. The estimation routine was repeated eight times: four times before and four times after adding the extra capacitor bank. Fig. 10 shows the estimated capacitance values and the calculated averages before and after the increase in the capacitance.

The averages of the estimated capacitance before and after the change in capacitance are 1.87 mF and 2.29 mF, respectively. Thus, the detected difference is 420 μF, which is close to the reference value 410 μF obtained at 100 Hz with the RLC meter (Philips PM6304).

In practice, long-term changes in the capacitance are slow in comparison with the identification time. However, if the capacitance were rapidly changed during the identification, the proposed linear model could not explain the identification results. Furthermore, this would cause a lower r^2 value as in the case of the varying load power (cf. Section IV-C). Moreover, the low r^2 value indicates that the estimation result is not correct, and gives a signal that identification should be repeated.

V. Conclusions

This paper presented a simple method for estimating the capacitance of the DC-link capacitor in three-phase voltage-source converters. The capacitance can be estimated during the startup routines of the converter or during the normal operation when the load power remains constant. The proposed method uses the typically available measurements of the DC-link voltage and phase currents of the converter, and no major changes are needed in the converter control algorithm. Thus, the method can be applied, e.g., in an active-front-end rectifier of a motor drive or in a solar inverter. The experimental results demonstrate that the capacitance is accurately estimated and the change in the capacitance is correctly detected. The results are shown for a three-phase converter, but the estimation principle could also be applied in the case of a different phase number or a converter topology.

ACKNOWLEDGMENT

The authors would like to thank ABB Oy, the Finnish Foundation for Technology Promotion, the Emil Aaltonen Foundation, and the Walter Ahlström Foundation for the financial support.

REFERENCES

[1] S. Yang, A. Bryant, P. Mawby, D. Xiang, L. Ran, and P. Tavner, "An industry-based survey of reliability in power electronic converters," *IEEE Trans. Ind. Appl.*, vol. 47, no. 3, pp. 1441–1451, May/Jun. 2011.

[2] K. Harada, A. Katsuki, and M. Fujiwara, "Use of ESR for deterioration diagnosis of electrolytic capacitor," *IEEE Trans. Power Electron.*, vol. 8, no. 4, pp. 355–361, Oct. 1993.

[3] H. Wang and F. Blaabjerg, "Reliability of capacitors for DC-link applications in power electronic converters – an overview," *IEEE Trans. Ind. Appl.*, vol. 50, no. 5, pp. 3569–3578, Sep./Oct. 2014.

[4] G. M. Buiatti, J. A. Martín-Ramos, A. M. R. Amaral, P. Dworakowski, and A. J. Marques Cardoso, "Condition monitoring of metallized polypropylene film capacitors in railway power trains," *IEEE Trans. Instrum. Meas.*, vol. 58, no. 10, pp. 3796–3805, Oct. 2009.

[5] A. Wechsler, B. C. Mecrow, D. J. Atkinson, J. W. Bennett, and M. Benarous, "Condition monitoring of DC-link capacitors in aerospace drives," *IEEE Trans. Ind. Appl.*, vol. 48, no. 6, pp. 1866–1874, Nov./Dec. 2012.

[6] M. Kim, S.-K. Sul, and J. Lee, "Condition monitoring of DC-link capacitors in drive system for electric vehicles," in *IEEE Vehicle Power and Propulsion Conference (VPPC 2012)*, Seoul, Korea, Oct. 2012, pp. 633–637.

[7] D.-C. Lee, K.-J. Lee, J.-K. Seok, and J.-W. Choi, "Online capacitance estimation of DC-link electrolytic capacitors for three-phase AC/DC/AC PWM converters using recursive least squares method," *IEE Proc. Electr. Power Appl.*, vol. 152, no. 6, pp. 1503–1508, Nov. 2005.

[8] A. G. Abo-Khalil and D.-C. Lee, "DC-link capacitance estimation in AC/DC/AC PWM converters using voltage injection," *IEEE Trans. Ind. Appl.*, vol. 44, no. 5, pp. 1631–1637, Sep./Oct. 2008.

[9] K.-W. Lee, M. Kim, J. Yoon, K.-W. Lee, and J.-Y. Yoo, "Condition monitoring of DC-link electrolytic capacitors in adjustable-speed drives," *IEEE Trans. Ind. Appl.*, vol. 44, no. 5, pp. 1606–1613, Sep./Oct. 2008.

[10] T. H. Nguyen and D.-C. Lee, "Deterioration monitoring of DC-link capacitors in AC machine drives by current injection," *IEEE Trans. Power Electron.*, vol. 30, no. 3, pp. 1126–1130, Mar. 2015.

[11] T. Alho, "Method and system for monitoring the condition of capacitors in a dc-voltage intermediate circuit," U.S. Patent US 8 829 919 B2, Sep. 9, 2014.

[12] K. Abdennadher, P. Venet, G. Rojat, J. M. Rétif, and C. Rosset, "A real-time predictive-maintenance system of aluminum electrolytic capacitors used in uninterrupted power supplies," *IEEE Trans. Ind. Appl.*, vol. 46, no. 4, pp. 1644–1652, Jul./Aug. 2010.

[13] A. Hatai, M. Unno, M. Daijou, and K. Eguchi, "Inverter device," U.S. Patent US 7 432 616 B2, Oct. 7, 2008.

[14] G. M. Buiatti, J. A. Martín-Ramos, C. H. R. García, A. M. R. Amaral, and A. J. Marques Cardoso, "An online and noninvasive technique for the condition monitoring of capacitors in boost converters," *IEEE Trans. Instrum. Meas.*, vol. 59, no. 8, pp. 2134–2143, Aug. 2010.

[15] R. Hoppler, U. Maier, D. Ryf, and L. Blahous, "A team of drives. Multidrives with active front-end technology in the cement and minerals industry," *ABB Review*, no. 3, pp. 30–34, Oct. 2008.

[16] M. Malinowski, M. Jasiński, and M. P. Kazmierkowski, "Simple direct power control of three-phase PWM rectifier using space-vector modulation (DPC-SVM)," *IEEE Trans. Ind. Electron.*, vol. 51, no. 2, pp. 447–454, Apr. 2004.

[17] T. Söderström and P. Stoica, *System Identification*. Hemel Hempstead, UK: Prentice Hall International, 1989.

[18] S. Chatterjee and J. S. Simonoff, *Handbook of Regression Analysis*. Hoboken, NJ, USA: John Wiley & Sons, 2013.

[19] V. Blasko, V. Kaura, and W. Niewiadomski, "Sampling of discontinuous voltage and current signals in electrical drives: a system approach," *IEEE Trans. Ind. Appl.*, vol. 34, no. 5, pp. 1123–1130, Sep./Oct. 1998.